



PII: S0010-938X(96)00031-5

## THE ENNOBLEMENT OF STAINLESS STEEL BY MANGANIC OXIDE BIOFOULING

W. H. DICKINSON,\* F. CACCAVO Jr and Z. LEWANDOWSKI

Center for Biofilm Engineering, 409 Cobleigh Hall, Montana State University, Bozeman, MT 59717, U.S.A.

**Abstract**—Twenty-three 316L stainless steel (SS) coupons were exposed *in situ* to fresh river-water for periods of up to 35 days. All samples developed steady-state corrosion potentials ( $E_{\text{corr}}$ ) near +350 mV (SCE) and polarization measurements showed enhanced cathodic current density characteristic of passive metal ennoblement. Epifluorescence and scanning electron microscopy of the attached biofilm showed numerous 10–20  $\mu\text{m}$  diameter Mn-rich annular deposits, associated clusters of bacterial cells, and abundant sheathed bacteria. Dissolution of the Mn deposits using  $\text{Na}_2\text{SO}_3$  shifted  $E_{\text{corr}}$  to pre-exposure values. SS coated with  $\text{MnO}_2$  paste displayed electrochemical behavior nearly identical to that of ennobled samples. A mechanism of ennoblement by  $\text{MnO}_2$  biofouling is proposed which explains a variety of findings on the electrochemical behavior of microbially colonized SS. Copyright © 1996 Published by Elsevier Science Ltd

**Keywords:** A. stainless steel, B. polarization, B. SEM.

### INTRODUCTION

Microbial colonization of passive metals can shift the corrosion potential ( $E_{\text{corr}}$ ) in the noble direction<sup>1–6</sup> and produce accompanying increases in current density and polarization slope at mild cathodic potentials.<sup>7–11</sup> The phenomena, collectively known as ennoblement, have been variously ascribed to depolarization of the oxygen reduction reaction,<sup>12,13</sup> acidification of the electrode surface,<sup>14</sup> the combined effect of elevated  $\text{H}_2\text{O}_2$  and decreased pH,<sup>6</sup> and the production of passivating siderophores.<sup>15</sup> Under marine conditions, ennobled potentials can exceed critical pitting potentials for low-molybdenum stainless steels,<sup>16</sup> and several cases of rapid loss of ennoblement have been attributed to localized corrosion.<sup>3,16</sup> Once initiated, pitting may proceed at accelerated rates due to the rapid cathodic reaction. These concerns have led to the use of elevated  $E_{\text{corr}}$  as an *in situ* diagnostic for potentially destructive microbial colonization of stainless steels.<sup>17</sup> Despite the notable technical impact of ennoblement, widespread efforts have made little progress in establishing the underlying mechanism.

In a previous report,<sup>18</sup> evidence was presented that ferric oxide abundance increases during ennoblement and the possibility was noted that ennoblement arises from changes in surface metal oxide properties. It is known that reduction of ferric oxides occurs simultaneously with oxygen reduction during mild cathodic polarization of iron,<sup>19</sup> indicating that ferric oxides can serve as cathodic depolarizers. As early as 1967 it was also shown that manganese oxides could be used to cathodically depolarize stainless steel under

strongly acidic conditions.<sup>20</sup> In these applications, galvanically coupled MnO<sub>2</sub> provided the high cathodic current density required for passivation in the acidic medium. Further, MnO<sub>2</sub> depolarization of stainless steel under alkaline conditions is a key characteristic in alkaline–manganese battery design.<sup>21–23</sup> Clearly, iron and manganese oxides may be expected to contribute to the cathodic current on stainless steel.

It is well known that iron and manganese oxides can be deposited by a variety of bacteria, including the sheathed bacteria *Leptothrix*<sup>24</sup> and the capsule-forming bacteria *Siderocapsa*.<sup>25</sup> Manganese-oxidizing bacteria are widely distributed in both marine and fresh waters, and have been investigated as a basis for biological removal of manganese from drinking water<sup>26</sup> and as a possible source of battery-grade manganese dioxide.<sup>27</sup> In aqueous environments, sheathed bacteria are responsible for tubercle formation on mild steels and allegedly promote severe pitting of stainless steel by production of aggressive ferric and manganic chlorides.<sup>28–30</sup> A possible direct role of MnO<sub>2</sub> in microbially influenced corrosion has been noted,<sup>31,32</sup> and massive structural failure due to microbial MnO<sub>2</sub> deposition has been reported.<sup>33</sup> Despite these considerations, the direct influence of microbially deposited MnO<sub>2</sub> on the electrochemical behavior of passive metals has received little attention.

The widespread natural abundance of manganese-oxidizing bacteria and the cathodic reactivity of MnO<sub>2</sub> suggest that the cathodic changes that occur during ennoblement may be due to MnO<sub>2</sub> biofouling. The goal of this paper is to demonstrate that manganic oxide biofouling can account for the electrochemical phenomenon of ennoblement.

## EXPERIMENTAL METHOD

A threefold approach was taken to assess the possible influence of MnO<sub>2</sub> biofouling on ennoblement: (1) biofilms on ennobled coupons were analysed for the presence of Mn; (2) the electrochemical properties of SS coated with a chemically prepared MnO<sub>2</sub> paste were determined and compared with those for ennobled coupons; and (3)  $E_{\text{CORR}}$  was monitored as MnO<sub>2</sub> was dissolved from coupon surfaces by chemical reduction with Na<sub>2</sub>SO<sub>3</sub>.

### In situ exposure

A set of 23 epoxy-embedded 316L SS coupons (UNS S31603; 1.59 cm diameter) were exposed to fresh, flowing stream-water at a field site near Bozeman, MT, by mounting the coupons in a 2 cm wide × 60 cm long open-channel polycarbonate reactor and submersing the reactor below the stream surface. Elemental composition of the coupons is given in Table 1. Mounting was such that a single face of each coupon was exposed in an inverted orientation that prevented suspended solids from settling onto the coupon surface. On the basis of chemical composition, the field site classifies as a clean stream (dissolved oxygen > 8 ppm; pH 8–8.5; alkalinity 3 meq l<sup>-1</sup>; nitrate ion 1.2 ppm; Ca<sup>2+</sup> 58 ppm; Mg<sup>2+</sup> 15 ppm;

Table 1. Elemental composition of 316L SS coupons (as provided by vendor, Metal Samples Inc. Munford, AL)

Composition (Wt %)									
C	Cr	Cu	Fe	Mn	Mo	Ni	P	S	Si
0.020	17.01	–	bal	1.71	2.12	11.08	0.035	0.002	0.60

$\text{Cl}^-$  3 ppm; dissolved Fe 200 ppb; conductivity  $4 \times 10^{-4} \text{ ohm}^{-1} \text{ cm}^{-1}$ ; total organic carbon 110 ppm). Temperature during the exposure was between 11 and  $15^\circ\text{C}$ , and dissolved Mn concentration was 10–20 ppb. Prior to the exposure, coupons were abraded on wet 600 grit silicon carbide paper, rinsed and sonicated in distilled water, rinsed with 95% ethanol, and air dried. In addition to the coupons, a set of glass microscope cover slips ( $18 \text{ mm} \times 18 \text{ mm} \times 1 \text{ mm}$ ) and several  $1 \text{ cm} \times 1 \text{ cm} \times 0.5 \text{ cm}$  pieces of reticulated vitreous carbon were exposed by submerging them approximately 50 cm upstream from the coupons at the field site. These materials were used to determine whether the metal substratum or dissolved metals from the stream water was the source of metal-rich microbial deposits, and to determine the influence of anodic passivation current on the limiting values of ennobled potentials.

$E_{\text{corr}}$  was measured vs the saturated calomel electrode (all potentials are reported vs the SCE) at roughly 1–3 day intervals. At these times, any accumulated material on the reactor floor was removed by flushing in stream water. While some solids typically settled on the reactor floor between flushings, these were never in contact with the coupons. For polarization measurements, samples were transported in stream water to the laboratory then cathodically polarized at  $-0.167 \text{ mV s}^{-1}$  in either filtered stream water or 0.01 M  $\text{Na}_2\text{SO}_4/\text{pH } 8.4$ , using a Princeton Applied Research model 273A potentiostat. The counter electrode was Pt foil ( $12.5 \text{ cm}^2$ ). Polarization curves carried out in the two media were indistinguishable. To determine the influence of oxygen on cathodic behavior, one sample was placed in argon-deaerated media for 30 min then polarized in the same deaerated media using the conditions given above. For these measurements, dissolved oxygen was measured using an Orion 97-08-00 dissolved-oxygen electrode.

### *Biofilm characterization*

The thickness of the microbial deposits was evaluated using reflected light microscopy by noting the travel of the calibrated stage adjustment while focusing first at the substratum then at the top of the deposits. Surface coverage was determined by directly measuring the cross-sectional area (footprint) of several annular deposits using a calibrated graticule, then counting individual annular deposits within a fixed area and multiplying by the average area of the deposits. Bacteria within the biofilm were visualized by staining for 1 to 2 min with a 0.1% (w/v) solution of acridine orange<sup>34</sup> followed by thorough rinsing with distilled water (DW), then viewing at either 400 or  $1000\times$  using an Olympus BH-2 epifluorescence microscope with 100 W Hg–UV source. Qualitative tests for the presence of  $\text{MnO}_2$  were based on development of the violet, oxidized form of leuco-crystal violet stain.<sup>35</sup> Briefly, 1 ml of 0.1% (w/v) leuco-crystal violet in 0.1 M  $\text{H}_2\text{SO}_4$  plus 2 ml 6 M acetic acid/acetate buffer at pH 4.0 were added to 7 ml DW and the resulting solution added dropwise to the material of interest. Acidified potassium ferrocyanide reagent<sup>25</sup> was used as a spot test for the presence of Fe(III) compounds. Morphology and elemental composition of the bacterial deposits were assessed by vapor-coating specimens with 15 nm of graphite and analysing, using a Jeol JSM-6100 scanning electron microscope with energy-dispersive X-ray analysis (SEM/EDS). Total Mn abundance in the biofilm was determined by scraping material from the coupons using a stainless steel razor blade, ashing 1 h at  $500^\circ\text{C}$ , digesting to dryness in hot, concentrated HCl, redissolving in 3 M  $\text{HNO}_3$ , and analysing at 279.5 nm using a Perkin–Elmer 3100 flame atomic absorption spectrophotometer.

Isolates of the naturally occurring Mn-oxidizing bacteria were obtained by streaking washed biofilm from the *in situ* exposed coupons onto a solid growth medium consisting of

1.0 g l<sup>-1</sup> peptone, 0.1 g l<sup>-1</sup> yeast extract, 0.5 g l<sup>-1</sup> MnSO<sub>4</sub>·H<sub>2</sub>O and 16 g l<sup>-1</sup> Bacto Agar in DW.<sup>26</sup> Single colonies were then restreaked to obtain pure cultures. The Mn-oxidizing capacity of these isolates was confirmed by the formation of a violet color on treatment with the leuco-crystal violet reagent.

### *MnO<sub>2</sub> studies*

The electrochemical behavior of MnO<sub>2</sub>-coated SS was investigated by physically applying MnO<sub>2</sub> paste to a portion of the coupon surface using a wooden applicator, then making  $E_{\text{corr}}$  and polarization measurements as described above. These coupons were not part of the *in situ* exposure. For some of these measurements, the roughly 1 mm thick paste coating was allowed to stand in contact with the coupon overnight, and was then wiped off with a cotton swab. This left a thin, brown, surface film covering the area where the paste coating had been applied, that was easily visualized by light microscopy. The thickness and surface coverage of the film were assessed as described for the biofilm deposits.

The MnO<sub>2</sub> paste was prepared by reduction of permanganate with manganous ion under alkaline conditions,<sup>36</sup> followed by repeated centrifugation and washing. The pH of the final MnO<sub>2</sub> suspension was 8.6. The paste was a finely divided material that produced a nearly continuous film when spread as a thin (< 10 μm) coating on glass or SS.

MnO<sub>2</sub> was also deposited electrochemically by anodically polarizing coupons at 3 mA cm<sup>-2</sup> for 20 s in a pH 6.4 solution containing 5 mM MnSO<sub>4</sub> and 0.1 M Na<sub>2</sub>SO<sub>4</sub>. The quantity of electrodeposited MnO<sub>2</sub> was determined from the duration of the potential plateau corresponding to MnO<sub>2</sub> reduction as the material was stripped from the surface by 10 μA cm<sup>-2</sup> constant cathodic current.

The influence of MnO<sub>2</sub> on  $E_{\text{corr}}$  for SS was determined by reductively dissolving the MnO<sub>2</sub>-rich deposits with sodium sulfite.<sup>37,38</sup> For these tests, ennobled coupons or coupons partially covered with chemically prepared MnO<sub>2</sub> were mounted in a rotating disk electrode and rotated at 300 rpm in 75 ml argon-deaerated 1.0 M Na<sub>2</sub>SO<sub>4</sub>/pH 8.4 while  $E_{\text{corr}}$  was continuously monitored. At a specified time, 75 ml 1.0 M Na<sub>2</sub>SO<sub>3</sub>/pH 8.5 was added while  $E_{\text{corr}}$  monitoring was continued. At the end of these tests, the electrolyte was removed and analysed for dissolved Mn by atomic absorption spectrophotometry. The rotating disk electrode was used to ensure a steady flux of reductant to the electrode and dispersion of soluble reaction products into solution.

## EXPERIMENTAL RESULTS

### *Electrochemical behavior*

$E_{\text{corr}}$  for the set of 23 coupons exposed *in situ* began to increase within 24 h of exposure and reached steady-state values near +350 mV within one to two weeks. Figure 1 shows data points for three samples from the set, depicting the varying rates of increase and illustrating that potentials for the coupons converge to a final value near +350 mV irrespective of the rate of increase. The shaded region in the figure envelopes the curves for all 23 coupons. For comparison,  $E_{\text{corr}}$  for a freshly prepared coupon, roughly one-third covered with a 100–200 μm thick layer of MnO<sub>2</sub> paste, is shown by the horizontal dashed line. Potential for this sample remained stable between +350 and +360 mV during a 24 h monitoring period following coating.

Figure 2 shows cathodic polarization behavior before exposure and after 160 and 500 h exposure for samples designated in Fig. 1. The marked increase in cathodic current density

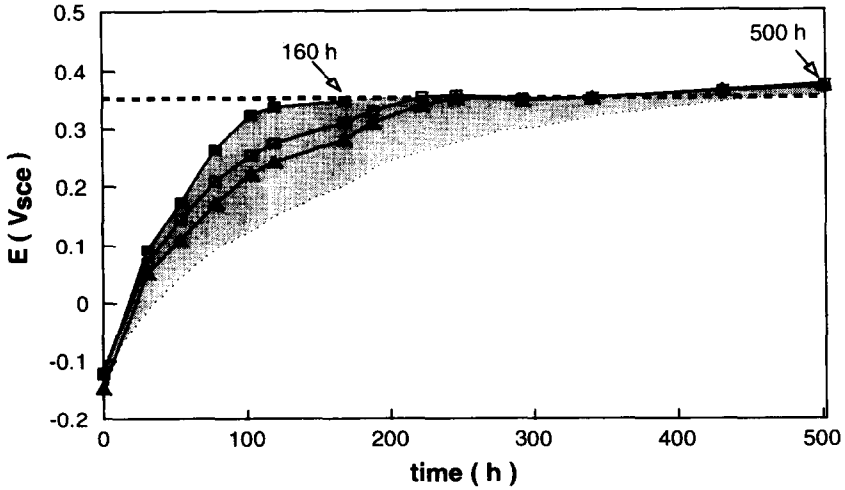


Fig. 1.  $E_{corr}$  vs time for 316L stainless steel coupons during *in situ* exposure to fresh river-water. Data points for 3 coupons used for polarization measurements are shown, while shaded area envelops curves for full 23-coupon set. At times denoted by arrows, cathodic polarization curves were measured. Horizontal dashed line indicates potential for  $MnO_2$  coated coupon.

at potentials above  $-300$  mV SCE, characteristic of ennoblement, is evident. It can also be seen that while  $E_{corr}$  remains nearly constant for the 160 and 500 h curves, current density at  $-200$  mV shows a threefold increase. This behavior is consistent with increasing surface coverage of the  $MnO_2$ -rich deposits, as will be explained in the discussion section. Figure 2

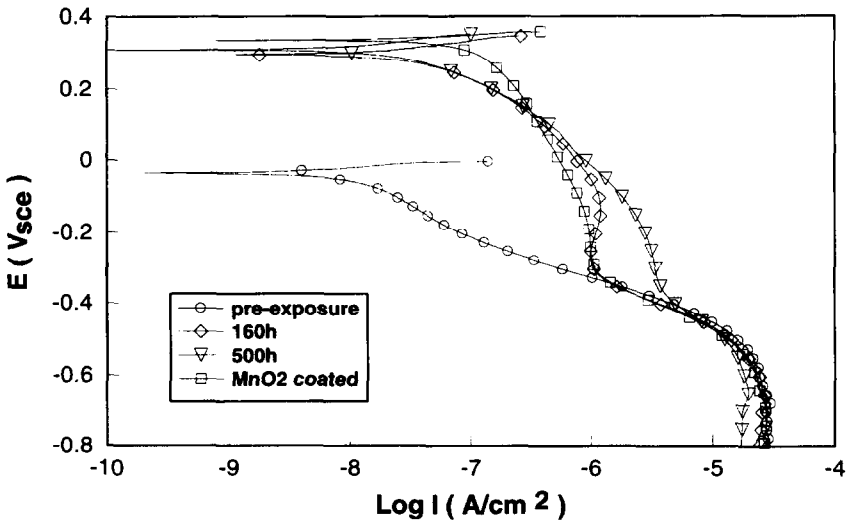


Fig. 2. Cathodic polarization curves for 316L SS coupons after different exposure intervals in fresh river-water, and for  $MnO_2$  coated coupon. Measurements were made in air saturated 0.01M  $Na_2SO_4$ /pH 8.4.

also shows polarization behavior for a coupon partially covered with an  $\text{MnO}_2$  film. The film, roughly  $10\ \mu\text{m}$  thick and covering about 6% of the coupon surface, was deposited by wiping off a thicker  $\text{MnO}_2$  paste coating that had been in contact with the coupon for 15 h. The similarity in polarization behavior for the  $\text{MnO}_2$ -coated and *in situ* exposed samples is evident.

To determine whether oxygen depolarization plays a role in ennoblement, as has frequently been proposed,<sup>5,8,10,12</sup> polarization curves in aerated and deaerated media were compared for the two coupons in Fig. 1 that displayed nearly identical  $E_{\text{corr}}$  behavior during 500 h exposure. The results, shown in Fig. 3, indicate that for potentials above  $-200\ \text{mV SCE}$ , where polarization changes associated with ennoblement are most apparent, oxygen reduction does not contribute significantly to cathodic current. Only at more negative potentials approaching the limiting current density does oxygen become the dominant cathodic reactant, as is illustrated by the diminished limiting current density of the deaerated curve. Dissolved oxygen concentration, measured in the reaction vessel before and after the deaerated run, was less than 0.1 ppm. These results rule out changes in the oxygen reduction rate as the cause of ennoblement under the conditions of this study.

#### *Biofouling deposits*

After 4 days' *in situ* exposure, one of the coupons, having an  $E_{\text{corr}}$  of  $+312\ \text{mV SCE}$ , was removed for microscopic examination of the biofilm. Inspection at  $400\times$  under reflected light revealed an abundance of isolated, annular, orange-brown deposits approximately  $10\text{--}20\ \mu\text{m}$  in diameter and up to  $3\ \mu\text{m}$  thick that covered about 10% of the coupon surface. These deposits stained blue when treated with Prussian Blue reagent, and violet on treatment with leuco-crystal violet, indicating the presence of  $\text{Fe(III)}$  compounds and  $\text{MnO}_2$ . Identical deposits were observed on glass cover slips exposed to the same environment.

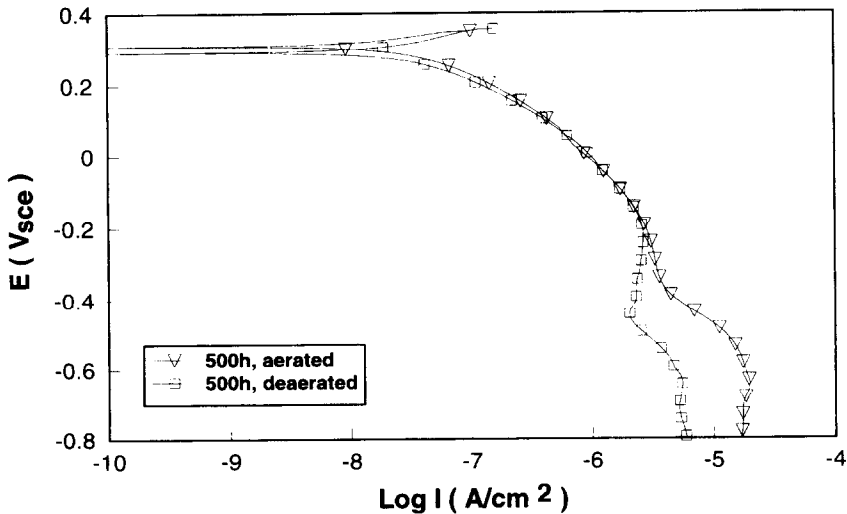


Fig. 3. Cathodic polarization curves in aerated and deaerated  $0.01\text{M Na}_2\text{SO}_4$ , pH 8.4, for 316L SS coupons after 500 h *in situ* exposure to fresh river-water.

Morphology and elemental composition of the annular deposits determined by SEM/EDS are shown in Figs 4 and 5, respectively. The deposits are distinctly ring-shaped with diameters slightly more than  $10\ \mu\text{m}$  and central voids  $3\text{--}4\ \mu\text{m}$  in diameter. Within the voids, the SS substratum is visible. SEM examination of coupons after 5 and 13 days' exposure showed no change in the physical appearance of the rings. However, the abundance as determined by light microscopy increased from about  $300\ \text{rings mm}^{-2}$  after 5 days, to about  $1100\ \text{rings mm}^{-2}$  after 23 days; the latter corresponds to 20% surface coverage.

Elemental mapping by EDS (Fig. 6) clearly shows the presence of manganese in the annular deposits, as well as calcium, carbon and oxygen, suggesting a mixed oxide/carbonate mineralogy as previously noted<sup>33</sup> for bulky deposits associated with massive pitting of stainless steel turbine blades. Total Mn in the biofilm after 14 days' exposure was  $1.6\ \mu\text{g cm}^{-2}$  or 0.2% by dry weight of the biofilm. Although iron was present within the annular deposits, as determined by Prussian Blue staining, detection by EDS was masked by a background signal from the metal substratum. Elemental maps for iron and chromium (not shown) indicated exposure of the substratum in the void area within the rings. Figure 5 shows the EDS spectrum of the ring for an interaction volume about  $2\ \mu\text{m}$  in extent, denoted by the arrow in Fig. 4. By comparison with the spectrum for the bare substratum (not shown), the only element detectable other than those already noted was magnesium. The carbon map shown in Fig. 6 suggests that the filament visible on the lower annular deposit of Fig. 4 may have been a bacterial sheath.

Epifluorescence microscopy of the acridine orange stained biofilm showed clusters of individual cells numbering from a few to several dozen within many of the annular deposits. A small cluster of four cells can be seen in the lower right portion of Fig. 7. Figure 7 also indicates the presence of distinct filamentous sheathed cells characteristic of iron and

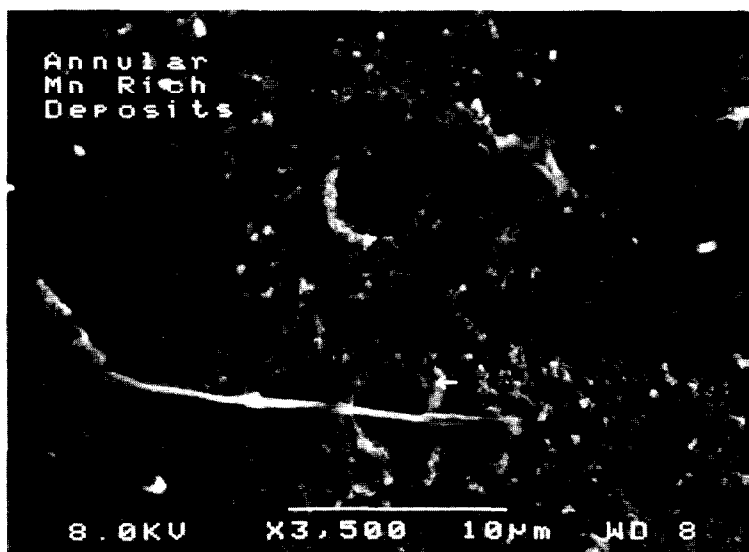


Fig. 4. SEM micrograph of annular deposits on SS coupon after 13 days' *in situ* exposure to fresh river-water. SS substratum is visible within the central void. Arrow indicates site for EDS spectrum shown in Fig. 5.

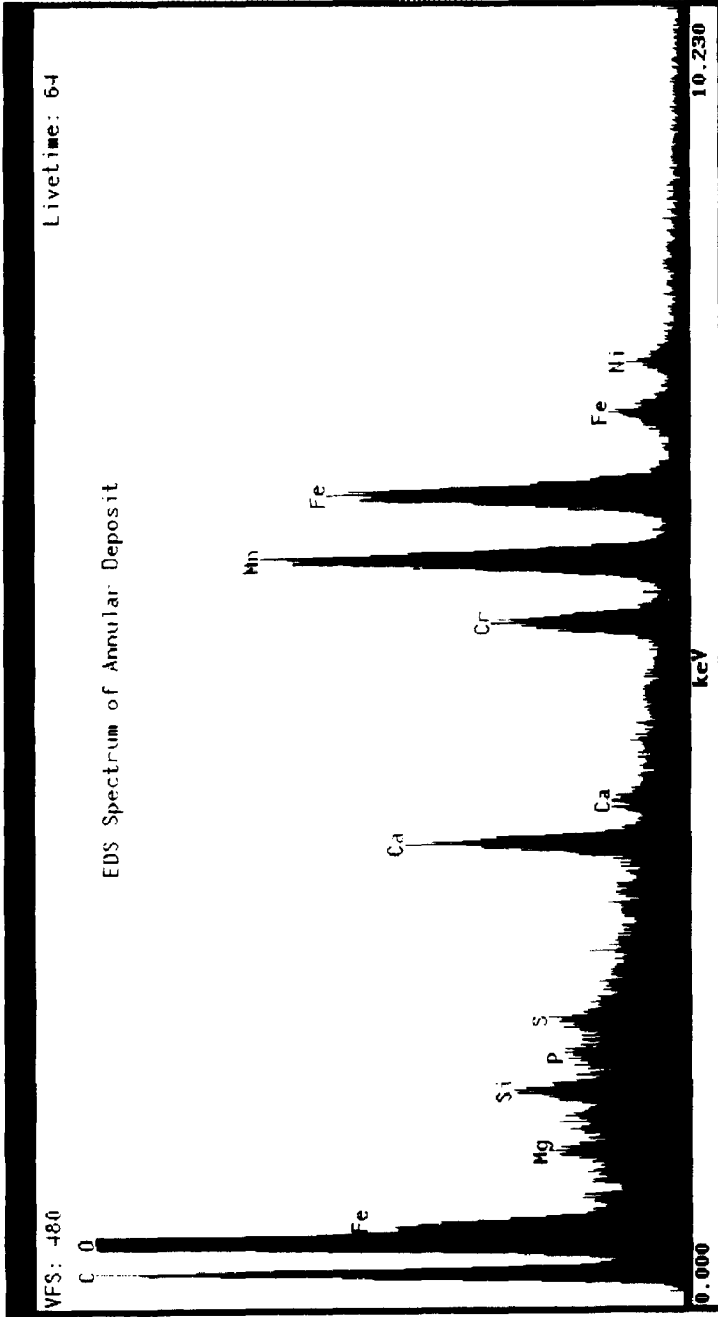


Fig. 5. EDS spectrum for annular deposit on SS coupon at site designated by arrow in Fig. 4. Spectrum shows the presence of Mn and Ca which were undetectable at an adjacent site on the exposed substratum.

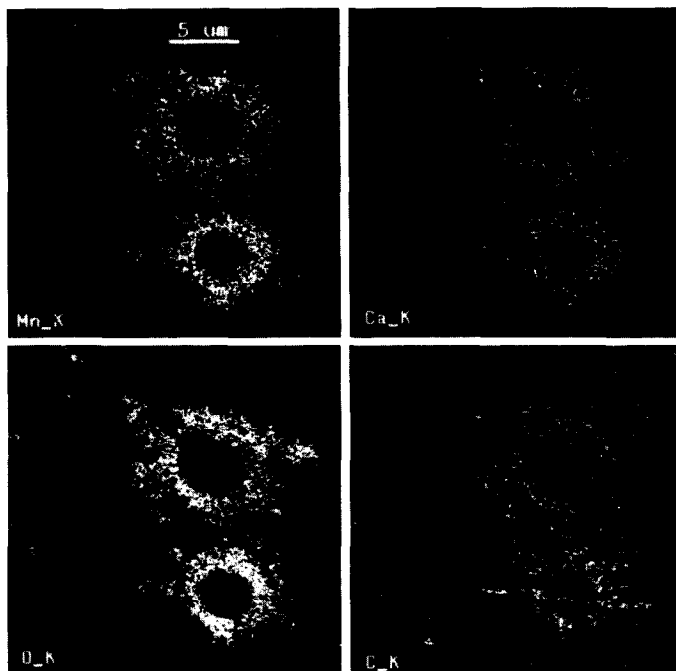


Fig. 6. EDS maps of region shown in Fig. 4 confirming the presence of Mn, Ca, O and C in the annular deposits.

manganese-oxidizing bacteria. Leuco-crystal violet staining of biofilms grown *in situ* on glass cover slips and viewed under phase contrast shows abundant manganic oxide deposits central to masses of radiating filamentous sheaths similar to the region visible in Fig. 7. These sheaths, as well as isolated cells, were abundant over the entire coupon surface. Both isolated subcultures of the filamentous bacteria and a separate isolate of sheath-free cells stained violet on treatment with leuco-crystal violet, indicating the presence of manganese-oxidizing bacteria within the biofilm. Morphology of the annular deposits seems suited to eventual capsule or microtubercle formation such as is exhibited by the genus *Siderocapsaceae*;<sup>25</sup> however, during the maximum exposure period of 5 weeks, neither encapsulation nor constriction of the area within the rings was observed.

#### *Sulfite dissolution experiment*

The influence of  $\text{MnO}_2$  deposits on  $E_{\text{corr}}$  was investigated by monitoring the potential as the deposits were reductively dissolved by sulfite ions (Fig. 8). The experiments were carried out in argon-deaerated media to minimize changes in  $E_{\text{corr}}$  arising from rapid and quantitative removal of dissolved oxygen by  $\text{SO}_3^{2-}$ . Dissolved oxygen measured prior to  $\text{SO}_3^{2-}$  addition was less than 0.01 ppm. In the first of three experiments, an *in situ* exposed coupon with an  $E_{\text{corr}}$  of +335 mV SCE and covered with numerous annular deposits was placed in deaerated medium and its potential was monitored for 3 h.  $E_{\text{corr}}$  decreased only slightly to +290 mV by the end of the period.

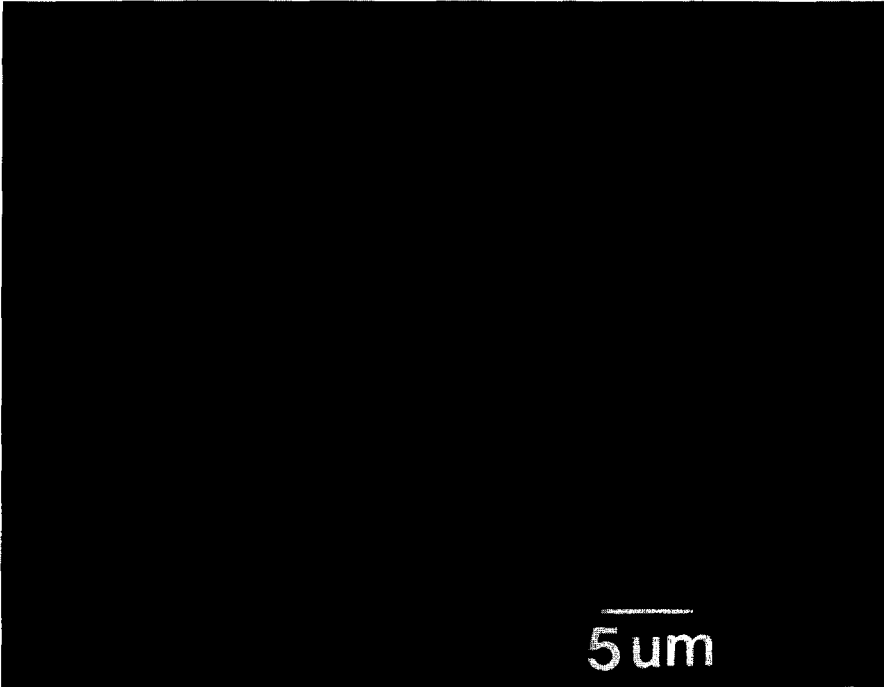


Fig. 7. Epifluorescence micrograph of acridine orange stained biofilm on SS coupon after 4 days' *in situ* exposure to fresh river-water. Individual bacterial cells centrally located within an Mn-rich annular deposit (lower right) as well as sheathed filamentous bacteria can be seen.

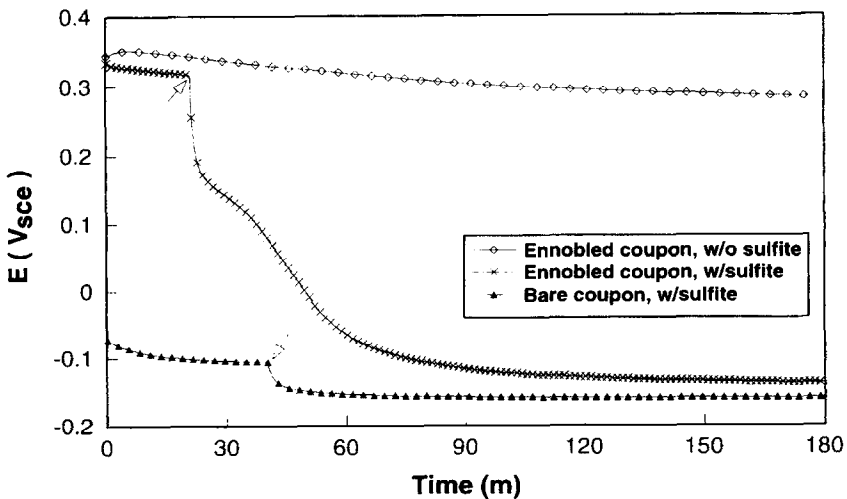


Fig. 8. Influence of 0.5M  $\text{SO}_3^{2-}$  on  $E_{\text{corr}}$  for 316L SS after 20 days' exposure to fresh river-water, and for unexposed coupon. Electrolyte was argon deaerated 0.5M  $\text{Na}_2\text{SO}_3^{2-}$  + 0.5M  $\text{Na}_2\text{SO}_4^{2-}$ , pH 8.4. Arrows denote time of sulfite addition.  $E_{\text{corr}}$  for a separate ennobled coupon in deaerated 1M  $\text{Na}_2\text{SO}_4^{2-}$ , pH 8.4, is also shown.

An unexposed coupon was placed in fresh deaerated medium, and  $E_{\text{corr}}$  was monitored for 40 min prior to making the solution 0.5 M in  $\text{SO}_3^{2-}$ . Addition of the  $\text{SO}_3^{2-}$  caused an abrupt potential decrease of approximately  $-50$  mV, after which  $E_{\text{corr}}$  remained stable at  $-150$  mV SCE. The origin of the potential decrease is not clear, but may have arisen from removal of residual dissolved oxygen or from polarization accompanying direct oxidation of  $\text{SO}_3^{2-}$  at the electrode surface. The latter explanation is consistent with a larger shift accompanying  $\text{SO}_3^{2-}$  addition to the ennobled sample (see below), insofar as  $\text{SO}_3^{2-}$  oxidation would be more rapid at the more positive potential.

An *in situ* exposed coupon with an  $E_{\text{corr}}$  of  $+330$  mV SCE and covered with numerous annular deposits was placed in fresh deaerated medium. After 20 min, during which  $E_{\text{corr}}$  decreased slightly to  $+310$  mV, the solution was made 0.5 M in  $\text{SO}_3^{2-}$ .  $\text{SO}_3^{2-}$  addition caused an abrupt drop in  $E_{\text{corr}}$  from  $+312$  mV to  $+170$  mV followed by a slower decrease to a near steady-state value of  $-140$  mV over the ensuing 90 min. The final value agrees well with typical  $E_{\text{corr}}$  values for 316L SS in neutral abiotic solution. Following treatment, the coupon surface was examined at  $400\times$  by reflected-light microscopy. All annular deposits had dissolved, and no evidence of mineral encrustation could be seen. Analysis of the electrolyte used in the experiment showed a manganese concentration of 80 ppb, corresponding to dissolution of  $6\ \mu\text{g cm}^{-2}$  of Mn from the coupon surface. In contrast, Mn concentration in solution from the first experiment was indistinguishable from blank levels.

The results of these experiments imply that the slow decrease in  $E_{\text{corr}}$  following  $\text{SO}_3^{2-}$  addition to the ennobled sample arose from gradual dissolution of the biomined MnO<sub>2</sub>, with  $E_{\text{corr}}$  approaching values characteristic of unexposed coupons as dissolution became complete. An identical experiment performed on an MnO<sub>2</sub>-film-coated coupon displayed similar results, with  $E_{\text{corr}}$  dropping abruptly from  $+250$  to  $+150$  mV on  $\text{SO}_3^{2-}$  addition, followed by a gradual decrease to a near steady-state value of  $-160$  mV over the ensuing 2 h.

### MnO<sub>2</sub> studies

Results of experiments in which MnO<sub>2</sub> paste was applied to the SS coupons are shown in Figs 1 and 2. The principal electrochemical effects of the MnO<sub>2</sub> coating were an increase in  $E_{\text{corr}}$  to a value virtually identical to the steady-state potential attained during *in situ* exposure, and an increase in cathodic current density at mild polarization, again quite similar to the changes exhibited by *in situ* exposed coupons. Both electrochemical characteristics were influenced by the amount of MnO<sub>2</sub> applied, the extent of surface coverage, and the duration of exposure. In general, less than 100  $\mu\text{g}$  of MnO<sub>2</sub> spread over approximately 20% of the coupon surface was sufficient to raise  $E_{\text{corr}}$  sharply to  $+350$  mV SCE. However, for such treatment, the potential began to decrease at rates of tens of  $\text{mV min}^{-1}$  after a few minutes' exposure, presumably due to MnO<sub>2</sub> discharge through the anodic passivation current. Application of thicker deposits, up to several  $\text{mg cm}^{-2}$ , caused no greater shift in  $E_{\text{corr}}$  but sustained the potential for periods up to several days. It was also observed that, by allowing the thicker deposits to remain in contact with the surface for several hours,  $E_{\text{corr}}$  remained stable at potentials near  $+350$  mV even after the bulk deposits were wiped off. Under these conditions, as little as a 10  $\mu\text{m}$  thick residual coating covering 6% of the surface was sufficient to maintain  $E_{\text{corr}}$  in excess of  $+320$  mV for several hours. These findings suggest that time of contact enhances discharge kinetics between the substratum and the cathodic material. This may explain the small

quantity of biofouling deposit (ca.  $1\text{--}2\ \mu\text{g (Mn) cm}^{-2}$ ) required to effect ennoblement, since, for *in situ* exposure, continued bacterial renewal of the  $\text{MnO}_2$  allows small quantities of material to remain in prolonged contact with the SS surface.

To obtain a better estimate of the amount of cathodically active  $\text{MnO}_2$  required to induce ennoblement, a thin, dark brown film of  $\text{MnO}_2$  was formed on several coupons by electrodeposition. It was assumed that electrodeposition would produce a coating of material in electrical contact with the substratum, whereas electrical continuity between the substratum and  $\text{MnO}_2$  paste coatings was expected to be less uniform. After the electrodeposition,  $E_{\text{corr}}$  was measured, and the deposit was then stripped from the surface by applying a constant cathodic current. The quantity (coulombs) of electroactive  $\text{MnO}_2$  was calculated from the duration of the potential plateau. It was found that  $E_{\text{corr}}$  attained near steady-state values of  $+280\ \text{mV}$  for deposition of  $8.5\ \text{mC cm}^{-2}$  of reducible  $\text{MnO}_2$  ( $4.8\ \mu\text{g (Mn) cm}^{-2}$  for a one-electron reduction). This is in fair agreement with the amount of Mn dissolved from the ennobled coupon in the  $\text{SO}_3^{2-}$  experiments ( $6\ \mu\text{g cm}^{-2}$ ); however, interpretation of the electrodeposition experiment is complicated by the undetermined effect of the strongly anodic deposition potential on the electrochemical behavior of the substratum.

The thickness and areal coverage of the synthetic  $\text{MnO}_2$  coatings also influenced the shape and current density of the cathodic polarization curves. Thin deposits ( $< 5\ \mu\text{m}$ ) covering more than about 20% of the surface frequently produced a current maximum of about  $3\ \mu\text{A cm}^{-2}$  near  $+50\ \text{mV SCE}$ . Similar peaks have been observed for ennobled coupons.<sup>9</sup> Polarization curves for thicker but less broadly distributed deposits did not produce such peaks (e.g. the  $\text{MnO}_2$  curve in Fig. 2), possibly because of incomplete reduction of the thicker deposits during the time-frame of the experiment.

## DISCUSSION

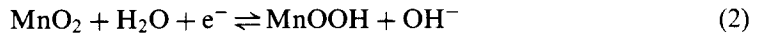
### *Mechanism of ennoblement by $\text{MnO}_2$*

The apparent limiting  $E_{\text{corr}}$  value of  $+350\ \text{mV SCE}$  attained during *in situ* exposure is in good agreement with the limiting potential range of  $+300$  to  $+400\ \text{mV}$  observed in the numerous studies on ennoblement.<sup>3-5,7-9</sup> The potential for  $\text{MnO}_2$  coated SS, as shown in Fig. 1, is virtually identical to this limiting potential, and the experiments indicate that once the minimum quantity of  $\text{MnO}_2$  paste required to attain  $+350\ \text{mV}$  is deposited, application of additional material causes no further increase in potential. The apparent potential limit for both these treatments suggests a limiting potential set by the reduction potential for  $\text{MnO}_2$  under the pH conditions of the experiments. At potentials below this value,  $\text{MnO}_2$  is thermodynamically unstable with respect to reduction and cathodically depolarizes the electrode, shifting  $E_{\text{corr}}$  in the noble direction. Polarization continues as additional  $\text{MnO}_2$  accumulation further enhances cathodic current, until the potential eventually stabilizes at the reversible  $\text{MnO}_2$  reduction potential. While anodic current from oxidation of the substratum may be expected to influence this steady-state potential, it was found that reticulated vitreous carbon, when coated with  $\text{MnO}_2$  paste or exposed at the field site, attained the same steady-state potential ( $+350\ \text{mV}$ ) that was shown by 316L SS. This indicates that the limiting potential in ennoblement reflects a reversible  $\text{MnO}_2$  couple rather than a mixed potential.

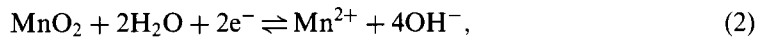
Although  $E_{\text{corr}}$  remains constant, continued accumulation of  $\text{MnO}_2$  causes cathodic current to increase at mild polarization, as shown for the 160 and 500 h curves in Fig. 2. As

noted in the experimental section, a current maximum is observed during cathodic polarization for some ennoblement studies and, in the present study, was observed at mild polarization for coupons more than about 20% covered with MnO<sub>2</sub> paste. These peaks may be essentially surface waves, as characteristically seen for voltammograms of adsorbed electroactive material,<sup>39</sup> that arise due to reduction of the MnO<sub>2</sub> surface deposits. For such conditions, peak current is proportional not only to surface coverage, which would explain the increasingly prominent peaks as surface coverage is increased, but to polarization sweep rate as well. Variations in the latter may explain the diversity of polarization curve shapes observed in different reports on ennoblement,<sup>5,9,10</sup> and may also provide the means to investigate electroactive surface coverage of the MnO<sub>2</sub> deposits. It is evident from Fig. 2 that cathodic polarization behavior of SS partially covered with an MnO<sub>2</sub> film can mimic that of microbially ennobled coupons very closely.

Although the electrochemistry of manganese oxides is complex, various arguments suggest that the well-known battery reaction<sup>40</sup>



may be the cathodic reaction in the above process. The reduction potential for this reaction at pH 8.0 and 25°C, based on  $\Delta G_f^\circ = -109.1 \text{ kcal mol}^{-1}$  for  $\gamma\text{-MnO}_2$ <sup>41</sup> and  $-133.3 \text{ kcal mol}^{-1}$  for  $\gamma\text{-MnOOH}$ ,<sup>41</sup> is +335 mV SCE, which is in good agreement with the observed value of +350 mV given the accuracy of  $\Delta G_f^\circ$  for these oxides. Furthermore, for such a solid phase reaction, the reduction potential is independent of dissolved Mn<sup>2+</sup> concentration. The variation in exposure conditions for ennoblement studies, including seawater, lake-water and river-water, and the expected seasonal cycling of [Mn<sup>2+</sup>],<sup>24</sup> would suggest greater variation in the limiting potential for ennoblement if a cathodic reaction involving Mn<sup>+2</sup>, such as



were operative. In addition, based on the *in situ* [Mn<sup>2+</sup>] of 0.3 μM measured in the present study, the reduction potential at pH 8.0 for reaction (2) is +235 mV. A manganese(II) concentration almost four orders of magnitude lower would be required to account for the observed potential of +350 mV. Although it must be noted that microbially induced changes in near-surface pH could shift reduction potentials for both reactions, previous microelectrode measurements on ennobled coupons made in this laboratory (unpublished data) showed no near-surface pH gradients. It is expected that measurements of  $dE_{\text{corr}}/d\text{pH}$  and  $dE_{\text{corr}}/d[\text{Mn}^{2+}]$  will aid in establishing the stoichiometry of the cathodic reaction that develops during ennoblement.

#### *Relationship to previous studies*

The proposed mechanism is consistent with a wide variety of published data on ennoblement. The electrochemical characteristics of synthetic MnO<sub>2</sub> deposits on SS are strikingly similar to those observed both in the present study and in the literature<sup>3-5,7-9</sup> for ennobled SS. In the only published report containing elemental analysis of biofilms on ennobled stainless steel, the presence of Mn (as well as oxygen and carbon) was noted,<sup>9</sup> while, in a separate report, EDS spectra show a complete absence of Mn<sup>42</sup> for microbially colonized stainless steel that failed to develop ennobled potential. Interestingly, in a related study on cathodic polarization behavior of stainless steel colonized by aerobic microorganisms, Mn was observed on coupons that developed marked cathodic

depolarization and pitting during colonization.<sup>43</sup> The occurrence of ennoblement in some studies but not in others has led to considerable debate concerning the conditions necessary for ennoblement.<sup>15,42,44</sup> In light of the proposed mechanism and the wide variability in abundance and redox state of Mn in natural waters, these different findings are not unexpected.

One of the most widely cited observations on ennoblement is the shift in  $E_{\text{corr}}$  to pre-exposure values that occurs when sodium azide is added to the biofilm on ennobled samples.<sup>2</sup> This finding has formed much of the basis for the proposed mechanisms of ennoblement involving electrocatalysis of the oxygen reduction reaction,<sup>2,5,10</sup> since it is assumed that sodium azide poisons extracellular enzymes or metalloporphyrin compounds that might otherwise catalyze charge transfer to oxygen. Results shown in Fig. 3 indicate, however, that oxygen is not the dominant depolarizer at modest cathodic potentials for ennobled SS. Furthermore, it has been established that sodium azide and other respiratory inhibitors suppress oxidative removal of  $\text{Mn}^{2+}$  from solution by suppressing microbial growth.<sup>26</sup> Thus the observed drop in  $E_{\text{corr}}$  on azide addition may have arisen from suppression of  $\text{MnO}_2$  deposition. Once microbial  $\text{MnO}_2$  production ceases, slow self-discharge of the previously accumulated material would eventually cause  $E_{\text{corr}}$  to decay. It is interesting that the drop in  $E_{\text{corr}}$  observed in the above study<sup>2</sup> was really quite slow, taking place over a period of 5 days; this is far longer than would be required for soluble electrocatalysts to diffuse away from the surface, but not an unreasonable time for passivation current densities of a few  $\text{nA cm}^{-2}$  to discharge a few  $\text{mC cm}^{-2}$  of  $\text{MnO}_2$ .

In other work on ennoblement, an apparent exponential temporal increase in cathodic current density at fixed potential was reported.<sup>8</sup> While this was ascribed to autocatalysis of the oxygen reduction reaction, Fig. 3 indicates that oxygen reduction does not control cathodic current at mild polarization for ennobled SS. In contrast, oxidation of  $\text{Mn}^{2+}$  to  $\text{MnO}_2$  is autocatalytic, insofar as adsorption of  $\text{Mn}^{2+}$  onto  $\text{MnO}_2$  dramatically increases the rate constant for oxidation.<sup>41</sup> Thus enhanced cathodic current due to biologically produced  $\text{MnO}_2$  will be augmented by an increasing rate of chemical  $\text{MnO}_2$  production as the deposit forms.

#### *Ennoblement and corrosion*

As noted in the introduction, a principal concern regarding passive metal ennoblement is the increased risk of localized corrosion that arises when  $E_{\text{corr}}$  exceeds the critical pitting potential of the metals. The morphology of the Mn-rich deposits that cause ennoblement in the present study may aggravate this concern. The typically ring-shaped deposits fix the site of the dominant cathodic reaction and, coupled with cell colonization within the rings, may provide ideal conditions for localized oxygen depletion, with consequent diminished redox potential. This would increase activation overpotential for the anodic reaction at the exposed substratum within the rings, and raise the risk of exceeding the critical pitting potential even beyond that anticipated by bulk solution chemistry. It is worth noting that such a scheme for localized attack does not require formation of ferric or manganic chlorides, although chloride would presumably compound the risk of attack.

Mn-rich microbial deposits have been implicated in the pitting of stainless steel turbine blades,<sup>33</sup> indicating that this type of fouling can cause severe material degradation. Given the number of reports on ennoblement, and the widespread distribution of manganese-oxidizing bacteria in natural waters, it is likely that conditions leading to  $\text{MnO}_2$  deposition and possible material failure are common. These conditions can be found in heat exchangers

and storage tanks where residual moisture following hydrostatic testing fosters bacterial growth.<sup>30</sup> Treatment for such fouling often includes mechanical disassembly and cleaning.<sup>45</sup> Although previous work has shown that physical removal of biofilm prevents ennoblement from occurring<sup>18</sup> and eliminates ennoblement once it has developed,<sup>9</sup> controlling ennoblement by this method will often be impractical or expensive. The mechanism proposed in this paper suggests that an alternative preventative measure may be to remove dissolved Mn(II) from influent water. This could be accomplished by chemical means, or by using methods established for biological removal of Mn(II) from drinking water;<sup>26</sup> the latter possibly providing a lower cost approach for large-volume cooling water requirements. In such a design, Mn(II) removal by microbial sand filters placed upstream from the target facility would lower the concentration sufficiently to prevent MnO<sub>2</sub> biomineralization downstream.

## CONCLUSIONS

Manganic oxide biofouling of 316L SS in fresh river-water shifts  $E_{\text{corr}}$  to steady-state values of +350 mV SCE, and increases cathodic current density at mild polarization by more than two orders of magnitude compared to unexposed samples. These electrochemical changes are very closely mimicked by the behavior of SS coupons partially coated with MnO<sub>2</sub> paste.  $E_{\text{corr}}$  exhibited during ennoblement agrees closely with the one-electron reduction potential for conversion of MnO<sub>2</sub> to MnOOH at the experimental pH. The origin of the Mn-rich deposits may be attributed to surface colonization by Mn-oxidizing bacteria.

Much of the data concerning ennoblement can be understood in terms of MnO<sub>2</sub> biofouling, including the correlation between ennoblement and the presence of Mn in biofilms, the influence of sodium azide on ennobled potential, and the autocatalytic nature of increasing cathodic current density that develops during microbial colonization. On the basis of the proposed mechanism of ennoblement, removal of dissolved Mn(II) from influent process waters may serve to prevent development of this potentially destructive microbial process.

*Acknowledgements*—This work was supported by the Office of Naval Research under the AASERT program, contract number N00014-92-J-1966, under ONR contract number N00014-95-1-0900, and by Cooperative Agreement EEC-8907039 between the National Science Foundation and Montana State University. SEM/EDS measurements were made at the Montana State University ICAL facility with the kind assistance of Nancy Equall.

## REFERENCES

1. A. Mollica, *4th Int. Congr. on Marine Corrosion and Fouling*, Antibes, France, p. 351 (1976).
2. V. Scotto, R. DiCintio and G. Marcenaro, *Corros. Sci.* **25**, 185 (1985).
3. S. C. Dexter and H. -J. Zhang, *11th Int. Corrosion Congr.*, Florence, Italy, p. 333 (1990).
4. A. Mollica, A. Trevis, E. Traverso, G. Ventura, G. DeCarolis and R. Dellepiane, *Corrosion* **45**, 48 (1989).
5. V. Scotto, M. Beggiano, G. Marcenaro and R. Dellepiane, *European Federation on Corrosion Publication 10*, p. 21 (1993).
6. P. Chandrasekaran and S. C. Dexter, *Corrosion/93*, Paper No. 493, Houston, TX, NACE (1993).
7. R. Holthe, P. O. Gartland and E. Bardal, *SINTEF Report No. STF16 A87123*. Trondheim, Norway (1987).
8. A. Mollica, *Int. Biodeterior. Biodegrad.* **29**, 213 (1992).
9. S. Motoda, Y. Suzuki, T. Shinohara and S. Tsujikawa, *Corros. Sci.* **31**, 515 (1990).
10. S. C. Dexter and G. Y. Gao, *Corrosion* **44**, 717 (1988).
11. R. Johnsen and E. Bardal, *Corrosion* **41**, 296 (1985).

12. A. Mollica, E. Traverso and G. Ventura, *European Federation on Corrosion Publication No. 10*, p. 149 (1993).
13. A. Mollica and G. Ventura, *Proc. 12th Int. Corrosion Congr.*, NACE, p. 3807 (1993).
14. S. Dexter and S.-H. Lin, *Proc. 7th Int. Congr. on Marine Corrosion and Fouling*, Valencia, Spain (1988).
15. M. Eashwar and S. Maruthamuthu, *Biofouling* **8**, 203 (1995).
16. H. H. Uhlig, *Corrosion and Corrosion Control*, 2nd Edn, p. 77. J. Wiley and Sons, New York (1971).
17. G. Licina, G. Nekoksa and G. Ward, *Int. Congr. on Microbially Influenced Corrosion and Biodeterioration*, Knoxville, TN, p. 5/41 (1990).
18. W. H. Dickinson and Z. Lewandowski, *Corrosion/95*, Paper No. 223, Houston, TX, NACE (1995).
19. E. R. Vago, E. J. Calvo and M. Stratmann, *Electrochim. Acta* **39**, 1655 (1994).
20. N. D. Tomashov and G. P. Chernova, *Passivity and Protection of Metals Against Corrosion*, p. 156. Plenum Press, New York (1967).
21. R. Okazaki, K. Morigaki, T. Ohhira, H. Fukuda, S. Kondo and Y. Matsuda, *Denki Kagaku* **62**, 975 (1994).
22. T. Hayasaka, T. Harada, T. Sakai and J. Ohshida, *European Patent Application* CODEN:EPXXDW (1993).
23. T. Ohira, T. Fujii, H. Fukuda and K. Ando, *Jpn. Kokai Tokkyo Koho* CODEN: JKXXAF (1986).
24. A.-M. Gounot, *FEMS Microbio. Rev.* **14**, 339 (1994).
25. H. Hanert, in *The Prokaryotes* (ed. M. Starr, H. Stolp, H. Truper, A. Balows and H. Schlegel), p. 1049. Springer-Verlag, Berlin (1981).
26. J. Vandenabeele, D. De Beer, R. Germonpre and W. Verstraete, *Microb. Ecol.* **24**, 91 (1992).
27. A. Greene and J. Madgwick, *Appl. Environ. Microbiol.* **57**, 1114 (1991).
28. G. Kobrin, *Mater. Perform.* **15**, 38 (1976).
29. D. Pope, D. Duquette, A. Johannes and P. Wayner, *Mater. Perform.* **23**, 14 (1984).
30. R. E. Tatnall, *Mater. Perform.* **20**, 41 (1981).
31. G. Kobrin, in *Biologically Induced Corrosion* (ed. S. Dexter), p. 33. NACE, Houston, TX (1986).
32. D. Duquette and R. Ricker, in *Biologically Induced Corrosion* (ed. S. Dexter), p. 121. NACE, Houston, TX (1986).
33. P. Linhardt, *Werks. Korr.* **45**, 79 (1994).
34. J. Hobbie, R. Daley and S. Jasper, *Appl. Environ. Microbiol.* **33**, 1225 (1977).
35. M. Kessick, J. Vuceta and J. Morgan, *Environm. Sci. Technol.* **6**, 642 (1972).
36. D. Lovley and E. Phillips, *Appl. Environ. Microbiol.* **54**, 1472 (1988).
37. A. Herring and S. Ravitz, *Soc. Mining Engineers* **00**, 191 (1965).
38. S. Asai, H. Negi and Y. Konishi, *Can. J. Chem. Eng.* **64**, 237 (1986).
39. A. Bard and L. Faulkner, *Electrochemical Methods, Fundamentals and Applications*, p. 522. Wiley and Sons, New York (1980).
40. R. Scarr and J. Hunter, in *Handbook of Batteries* (ed. D. Linden), p. 10. 1. McGraw-Hill, New York (1995).
41. W. Stumm and J. J. Morgan, *Aquatic Chemistry*, p. 526. Wiley-Interscience (1970).
42. B. J. Little, R. Ray, P. Wagner, Z. Lewandowski, W. C. Lee, W. G. Characklis and F. Mansfeld, *Biofouling* **3**, 45 (1991).
43. B. Little, P. Wagner and D. Duquette, *Corrosion* **44**, 270 (1988).
44. F. Mansfeld and B. Little, *Corrosion* **45**, 786 (1989).
45. R. Tatnall, *Mater. Perform.* **20**, 32 (1981).